

Fine-grained Data Distribution Alignment for Post-Training Quantization

Yunshan Zhong¹, Mingbao Lin¹, Mengzhao Chen¹, Ke Li³, Yunhang Shen³, Fei Chao¹, Yongjian Wu³, Feiyue Huang³, Rongrong Ji^{1,2*}

¹Media Analytics and Computing Lab, Department of Artificial Intelligence,
School of Informatics, Xiamen University

²Institute of Artificial Intelligence, Xiamen University
³Tencent YouTu Lab

Abstract

While post-training quantization receives popularity mostly due to its evasion in accessing the original complete training dataset, its poor performance also stems from this limitation. To alleviate this limitation, in this paper, we leverage the synthetic data introduced by zero-shot quantization with calibration dataset and we propose a fine-grained data distribution alignment (FDDA) method to boost the performance of post-training quantization. The method is based on two important properties of batch normalization statistics (BNS) we observed in deep layers of the trained network, *i.e.*, inter-class separation and intra-class incohesion. To preserve this fine-grained distribution information: 1) We calculate the per-class BNS of the calibration dataset as the BNS centers of each class and propose a BNS-centralized loss to force the synthetic data distributions of different classes to be close to their own centers. 2) We add Gaussian noise into the centers to imitate the incohesion and propose a BNS-distorted loss to force the synthetic data distribution of the same class to be close to the distorted centers. By introducing these two fine-grained losses, our method shows the state-of-the-art performance on ImageNet, especially when the first and last layers are quantized to low-bit as well. Our project is available at <https://github.com/viperit/FDDA>.

Introduction

Recent years have witnessed the rising of deep neural networks (DNNs) in computer vision, natural language processing, and many other domains. Despite the tremendous success of DNNs, the increasing model size significantly barricades the deployment of DNNs on many resource-limited platforms such as mobile phones, embedding devices, *etc*. To overcome this dilemma, varieties of methods (Han et al. 2015; Krishnamoorthi 2018) are explored to reduce the complexity of DNNs. Network quantization, which represents full-precision DNNs in a low-precision format, emerges as a promising direction (Krishnamoorthi 2018; Banner et al. 2019; Lin et al. 2020).

By tuning the quantized DNNs using a small calibration dataset, post-training quantization, a sub-topic of low-precision quantization, has received very favorable attention from both academia and industries. Recent studies show that

a post-training quantized model in high precision such as 8-bit can reach performance on par with the full-precision version (Krishnamoorthi 2018; Banner et al. 2019). However, severe performance degradation occurs while quantized to lower precision such as 4-bit (Li et al. 2021). For example, as reported in LAPQ (Nahshan et al. 2019), quantizing ResNet-18 (He et al. 2016) to 8-bit can well retain the accuracy of the full-precision network (around 71.5%), but only 60.3% top-1 accuracy can be observed when quantized to 4-bit. To alleviate this problem, varieties of studies are explored to enhance low-bit performance. The mainstream can be outlined into two folds. The first group designs sophisticated quantization methods such as linear combination of multiple low-bit vectors (Liu et al. 2021), weight region separation (Fang et al. 2020), mixed-precision quantization (Liu et al. 2021), partial quantization (Kryzhanovskiy et al. 2021) and so on. The second group reformulates the rounding function or loss constraints from an analytical perspective. For example, (Nagel et al. 2020) derived an adaptive rounding by modeling rounding problem as quadratic constrained binary optimization. (Li et al. 2021) showed that the best output reconstruction lies in a block unit via the second-order analysis of reconstructing intermediate outputs.

Though great efforts have been made, improvements of these studies are still limited. Besides, the performance gains are usually built on the premise that the first and last layers are quantized to 8-bit (Hubara et al. 2020; Wang et al. 2020), or even retained in full-precision states (Nahshan et al. 2019; Nagel et al. 2020). However, severe performance degradation occurs when all layers are quantized to very low-bit integers (see Tab. 1). We step back and think about the root cause of significant accuracy degradation in post-training quantization. We attribute it to a lack of training data. Specifically, the low-bit network bears poor representation ability, and a very small calibration dataset cannot support the quantized model to fit well the real data distribution. Many researches on zero-shot quantization are indicated to synthesizing fake images using data optimizer (Cai et al. 2020; Haroush et al. 2020) or data generator (Xu et al. 2020; Zhang et al. 2021a). The synthetic data is then used to train the quantized model. Though this manner partly alleviates data lacking, performance drops greatly if simply using synthetic data. For example, (Li et al. 2021) observed only 21.71% top-1 accuracy when quantizing ResNet-18 to 4-bit in a sin-

*Corresponding Author: rrji@xmu.edu.cn

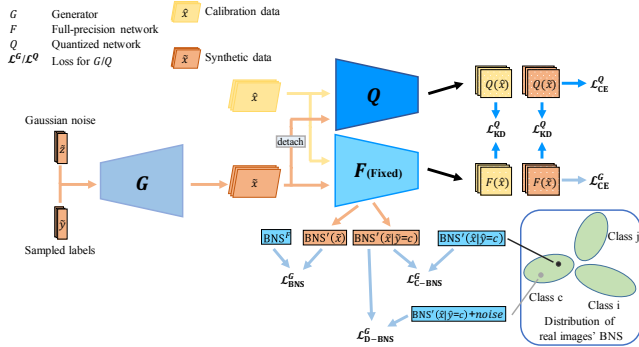


Figure 1: Framework of our FDDA. We deploy a generator G to produce synthetic data supervised by the coarse BNS alignment loss ($\mathcal{L}_{\text{BNS}}^G$), and two proposed fine-grained distribution losses ($\mathcal{L}_{\text{C-BNS}}^G$ and $\mathcal{L}_{\text{D-BNS}}^G$).

gle zero-shot manner (Cai et al. 2020). So far, combining real calibration dataset with synthetic data remains unexplored in post-training quantization, and we believe, might be a promise of boosting the low-bit performance.

Motivated by the above analyses, in this paper, we propose fine-grained data distribution alignment (termed FDDA) for post-training quantization, as illustrated in Fig. 1. FDDA is inspired by the fact that the representation of synthetic data has been demonstrated to be feasible in many other tasks such as image super-resolution (Zhang et al. 2021b), light-weight student network (Chen et al. 2019) and zero-shot quantization (Xu et al. 2020), and for the first time, we apply it to post-training quantization to tackle the insufficient data problem, providing a new perspective for post-training quantization. Following (Xu et al. 2020), we make full use of the pre-trained model to guide the generator to synthesize fake data. Except for the distillation of output logits between the pre-trained model and its quantized version to improve the quantization performance, (Xu et al. 2020) proposed to retain the distribution information of training data, modeled by the batch normalization statistics (BNS) in the pre-trained model. To this end, the mean and variance of the synthetic data distribution are constrained to be the same as these of the real data distribution. However, we realize that, based on our two insightful observations on BNS, this information retaining manner is very coarse for deep layers.

Specifically, we calculate the mean and variance *w.r.t.* each image sample and the statistical results are visualized in Fig. 2. As can be observed, the BNS of different classes are overlapping in shallow layers. However, two properties of deep BNS are observed including inter-class separation and intra-class incohesion. The former indicates different classes possess varying BNS while the latter indicates a small distortion of BNS among data from the same class. The BNS captured in the pre-trained model only reflects the distribution of the whole dataset, which are applicable to shallow layers with mixed class-wise BNS. However, these BNS in the pre-trained model are very coarse for deep layers with separable class-wise BNS. Thus, the synthetic data needs a fine-grained BNS alignment for these deep layers.

To this end, we further introduce a BNS-centralized loss

and a BNS-distorted loss, respectively to align the fine-grained BNS properties of inter-class separation and intra-class incohesion. In contrast to zero-shot quantization (Cai et al. 2020), an additional calibration dataset, usually comprising one image per class, can be available in post-training quantization. To fully utilize this bonus, we derive means and variances of each image in deep layers of the pre-trained model, and then define the computed means and variances as the BN centers of each class. To preserve inter-class separation, our BNS-centralized loss forces the synthetic data distributions of different classes closely to their own centers. To preserve intra-class incohesion, we add Gaussian noise into the centers to imitate the distortion and the BNS-distorted loss forces the synthetic data distribution of the same class closely to the distorted centers. Through a fine-grained BNS alignment, our proposed FDDA significantly improves the quantization performance over existing methods on ImageNet (Li et al. 2021; Wang et al. 2020; Hubara et al. 2020), particularly when the first and last layers are also quantized to low-bit. Our contributions are three-fold:

- To our best knowledge, we are the first to explore combining calibration dataset with synthetic data in post-training quantization, which might provide a new perspective for post-training quantization.
- We observe properties of inter-class separation and intra-class incohesion in deep BNS. Besides, we devise a BNS-centralized loss and a BNS-distorted loss to preserve these two properties in synthetic data.
- Extensive experiments demonstrate that our FDDA can well improve the performance on ImageNet. For example, our FDDA outperforms the current SOTA, BRECQ (Li et al. 2021), by 6.64% in the top-1 accuracy when all layers of MobileNet-V1 are quantized to 4-bit.

Related Work

In this section, we briefly discuss the most related work to ours including post-training quantization and zero-shot quantization. A more comprehensive survey can be referred to (Gholami et al. 2021).

Post-training Quantization. Most existing post-training quantization methods attempt to alleviate the accuracy deterioration problem from two perspectives: designing more sophisticated quantization methods and introducing a new rounding function or loss function. From the first perspective, (Liu et al. 2021) proposed to close the gap between the full-precision weight vector and its low-bit version by using the linear combination of multiple low-bit vectors. (Wang et al. 2020) finished quantization in a two-stage manner of bit-split and bit-stitching. In the bit-split stage, the K -bit constraint of integer is split into $(K-1)$ ternary learning problems, and each bit is then separately solved in an iterative optimization procedure. In the bit-stitching stage, the K -bit integer is recovered by the linear combination with a base of 2^{k-1} for the k -th bit. In addition, they also use channel-wise quantizer for activations and integrate the scaling factor into corresponding 2D kernels to avoid extra storage. Piece-wise linear quantization (Fang et al. 2020) splits

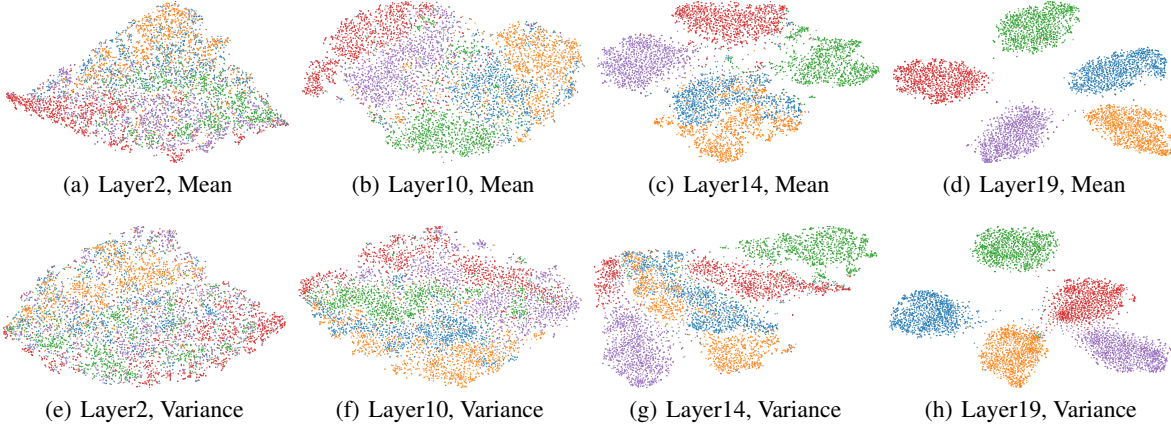


Figure 2: t-SNE visualization (five classes) of BNS in different layers of pre-trained ResNet-18 on ImageNet. BNS in shallow layers are overlapping. For deep layers, different classes have varying BNS and there exists small distortion within data from the same class. Similar observations can be found in other networks as well. Best viewed in color.

the whole weights into two non-overlapping areas, including one dense region comprising low-magnitude weights, and one sparse region comprising high-magnitude weights. On top of the splitting, both areas are respectively quantized into the same low-bit. To model the quantization parameters, (Kryzhanovskiy et al. 2021) constructed a linear regressor to predict the α -quantile of activations, which eliminates the involvement of complex sorting algorithm. From the second perspective, AdaRound (Nagel et al. 2020) analyzes that it is not advisable to simply round full precision weight to its nearest fixed-point value. Alternatively, the rounding problem is formulated as a per-layer quadratic unconstrained binary optimization problem, based on which, a continuous relaxation is introduced to find an adaptive rounding. BRECQ (Li et al. 2021), one of the state-of-the-art methods, builds a block-wise reconstruction between the outputs of the full precision network and quantized network to achieve a balance between cross-layer dependency and generalization error. Besides, trainable clipping (Choi et al. 2018) for activations is also considered by BRECQ. Similar motivation can also be found in earlier works (Hubara et al. 2021; Wang et al. 2020; Banner et al. 2019).

Zero-Shot Quantization. Zero-shot quantization is not permitted to access the training dataset. Thus, synthetic samples become an alternative to calibrate and fine-tune the quantized models. According to the methodology of data synthesis, we categorize existing studies into two groups: data optimizer (Cai et al. 2020; Haroush et al. 2020) and data generator (Xu et al. 2020; Zhang et al. 2021a; Liu, Zhang, and Wang 2021). Data optimizer based methods produce synthetic images from Gaussian noise. (Cai et al. 2020) forward propagated the Gaussian inputs to collect BNS. Then the optimization that minimizes the difference between the collected BNS and the BNS in the pre-trained model is constructed to update the Gaussian inputs to ensure that the synthetic data does not deviate from the real data distribution. Except for aligning the BNS, (Haroush et al. 2020) further introduced a Domain Prior loss and an Inception loss. The former encourages nearby pixels between the input image and its Gaussian-smoothed variant to be similar. The lat-

ter prevents the model from producing inputs that lead to exploding outputs. As for data generator, this group is featured with a generator in Generative Adversarial Networks (GAN) (Goodfellow et al. 2014) to synthesize images. (Xu et al. 2020) exploited the classification boundary knowledge and distribution information in the pre-trained model, and then devised a knowledge matching generator to produce synthetic data for model quantization. To break the data homogenization, DSG (Zhang et al. 2021a) slacks the alignment of BNS and introduces a layer-wise enhancement to enhance diverse data samples. On the contrary, (Liu, Zhang, and Wang 2021) designed a two-level discrepancy modeling to diversify generated data in an adversarial fashion.

Methodology

Preliminaries

Quantizer. Following (Cai et al. 2020; Xu et al. 2020), we adopt asymmetric uniform quantization in this paper. Given the data \mathbf{x} (weights or activations), bit-width b , lower bound l and upper bound u , the quantizer is defined as:

$$\mathbf{q} = \text{round}\left(\frac{\text{clip}(\mathbf{x}, l, u)}{s}\right), \quad (1)$$

where $\text{clip}(\mathbf{x}, l, u) = \min(\max(\mathbf{x}, l), u)$, $\text{round}(\cdot)$ rounds its input to the nearest integer, $s = \frac{u-l}{2^b-1}$ is the scaling factor that projects a floating-point number to a fixed-point integer, and \mathbf{q} is the quantized fixed-point number. The corresponding de-quantized item $\bar{\mathbf{x}}$ can be obtained as:

$$\bar{\mathbf{x}} = \mathbf{q} \cdot s. \quad (2)$$

For activations and weights, we use layer-wise quantizer and channel-wise quantizer respectively. The lower bound l and upper bound u are set to the minimum and maximum of per-layer activations (per-channel weights).

Data Synthesis. Ideally, post-training quantization completes network compression with a small calibration dataset $D = \{(\hat{\mathbf{x}}, \hat{y})\}$, typically consisting of one image per class¹.

¹Sometimes, the label \hat{y} is not available. Nevertheless, it can be predicted by the pre-trained full-precision model.

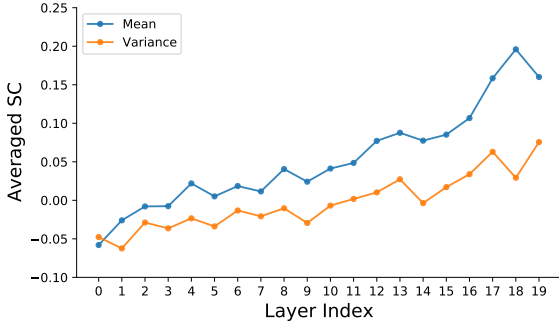


Figure 3: The Average of Silhouette Coefficient values *w.r.t.* the BNS in different layers.

However, this small calibration dataset fails to retain performance when quantizing the network to very low precision, such as 4-bit. Inspired by zero-shot quantization, we resort to data synthesis. As shown in Fig. 1, we deploy a generator G to synthesize an image \tilde{x} from a random Gaussian noise \tilde{z} conditioned on the target label \tilde{y} , *i.e.*, $\tilde{x} = G(\tilde{z}|\tilde{y})$. We expect that the synthetic data to be similar to the real data. Despite the inaccessibility of the whole training data, we can turn to the data distribution information captured by the batch normalization statistics (BNS) in the pre-trained model F . Following (Xu et al. 2020), the BNS loss can be adopted to preserve the distribution:

$$\mathcal{L}_{\text{BNS}}^G = \sum_{l=1}^L \|\mu'_l(\tilde{x}) - \mu_l^F\|^2 + \|\sigma'_l(\tilde{x}) - \sigma_l^F\|_2^2, \quad (3)$$

where μ_l^F and σ_l^F are the running mean and variance in the l -th layer of pre-trained F . $\mu'_l(\cdot)$ and $\sigma'_l(\cdot)$ return the mean and variance of input data in the l -th layer of F .

Classification. We also use cross-entropy loss to ensure synthetic data can be correctly classified by the pre-trained model F :

$$\mathcal{L}_{\text{CE}}^G = \mathbb{E}_{(\mathbf{x}, y) \sim \{(\tilde{x}, \tilde{y})\}} [\text{CE}(F(\mathbf{x}), y)]. \quad (4)$$

Note that, we fix F during the whole training process, and the generator G is updated instead.

Our Insights

The BNS in pre-trained F are computed by a series of averages of different batches of the full training set, *a.k.a.*, moving average. As a consequence, they capture the distribution of the whole dataset. However, it is unclear whether they can be a representative of per-class BNS or even per-image BNS. To verify this, we feed the whole ImageNet to ResNet-18 (He et al. 2016) and calculate per-image mean vector μ'_l and variance vector σ'_l in each layer. Fig. 2 visualizes some examples via t-SNE (van der Maaten and Hinton 2008).

As can be seen, the BNS over different classes vary a lot across different layers. Specifically, the BNS of different classes are overlapping in shallow layers while there is regularity in deep layers, which can be outlined into two properties: **inter-class separation** and **intra-class incohesion**. The former indicates that the BNS within the same class are formed into one cluster and different classes are

separable. The latter refers to a small distortion of BNS among data from the same class. To quantitatively measure these two properties, we introduce Silhouette Coefficient (SC) (Rousseeuw 1987), a value of which reflects how similar an object is to its own cluster (cohesion) in comparison with other clusters (separation). SC value of one sample \mathbf{v} is defined as:

$$\text{SC}(\mathbf{v}) = \frac{b(\mathbf{v}) - a(\mathbf{v})}{\max(a(\mathbf{v}), b(\mathbf{v}))}, \quad (5)$$

where $a(\mathbf{v})$ denotes the average of intra-cluster distance for sample \mathbf{v} . And $b(\mathbf{v})$ is the average of nearest-cluster distance for sample \mathbf{v} . Note that $b(\mathbf{v})$ is the distance between \mathbf{v} and the nearest cluster that \mathbf{v} is not a part of. The value of $\text{SC}(\mathbf{v})$ ranging from -1 (separation) to +1 (cohesion). Values near 0 indicate overlapping clusters. Negative values generally indicate that a sample has been assigned to the wrong cluster, as a different cluster is more similar. Using Eq. (5), we can obtain SC values for each mean vector μ'_l and variance vector σ'_l . Fig. 3 displays the average of all input samples in each layer. As can be seen, the SC values are very small, even negative, in shallow layers, which indicates overlapping clusters. On the contrary, SC values increases in deep layers, which indicates inter-class separation. However, the increase of SC is very limited (no more than 0.25), which indicates a relatively large intra-cluster distance, *i.e.*, intra-class incohesion. These analyses are consistent with the observations in Fig. 2.

In-depth Analysis. The observed inter-class separation and intra-class incohesion, we believe, can be explained by the fact that networks extract class-unrelated universal low-level features in shallow layers such as edges and curves. While in deep layers, networks are learned to extract class-related semantic features distinguishable from other classes in deep layers, leading to inter-class separation. The intra-class incohesion results from the varying image contents though these images are from the same class. For shallow layers, the overlapping clusters hardly model a subtle per-class distribution thus the BNS in the pre-trained model can be an alternative. However, the BNS in the pre-trained model are very coarse and the constraint of Eq. (3) cannot model the properties of per-class separation and intra-class incohesion. Thus, apart from the coarse-grained alignment, a fine-grained BNS alignment is also necessary for deep layers.

Fine-grained BNS Alignment

To preserve the properties of inter-class separation and intra-class incohesion, in this subsection, we respectively introduce a BNS-centralized loss and a BNS-distorted loss. Details are presented below.

BNS-centralized Loss. Since the BNS of each class are formed into one cluster, we can place a centroid as an explicit supervisory signal for each class and force the per-class distribution of synthetic images to be close to the assigned centroid. Recall that a real image (\hat{x}, \hat{y}) per class can be available from the calibration dataset D in post-training quantization. It is reasonable to use the BNS of image \hat{x}

as the corresponding centroid of class \hat{y} since its BNS already fall into the target cluster and are separable from BNS of other classes. To this end, given $\tilde{\mathbf{x}}$ with its label $\tilde{y} = c$, we define the following BNS-centralized loss such that synthetic images can be further aligned to their corresponding centroids:

$$\mathcal{L}_{\text{C-BNS}}^G = \sum_{l=K}^L \|\boldsymbol{\mu}'_l(\tilde{\mathbf{x}}|\tilde{y} = c) - \boldsymbol{\mu}'_l(\hat{\mathbf{x}}|\hat{y} = c)\|^2 + \|\boldsymbol{\sigma}'_l(\tilde{\mathbf{x}}|\tilde{y} = c) - \boldsymbol{\sigma}'_l(\hat{\mathbf{x}}|\hat{y} = c)\|^2, \quad (6)$$

where K is a pre-given hyper-parameter denoting the start of deep layers. In the experiments, we set $K = \text{ceil}(\frac{L}{2}) - 2$ where $\text{ceil}(\cdot)$ is the rounding up function.

BNS-distorted Loss. Our BNS-centralized loss ensures the fine-grained separability across different classes. However, how to retain the incohesion within the same class remains an issue. To solve this, we further propose to distort the centroid of per-class BNS by introducing Gaussian noise and define the following BNS-distorted loss:

$$\mathcal{L}_{\text{D-BNS}}^G = \sum_{l=K}^L \|\boldsymbol{\mu}'_l(\tilde{\mathbf{x}}|\tilde{y} = c) - \mathcal{N}(\boldsymbol{\mu}'_l(\hat{\mathbf{x}}|\hat{y} = c), \boldsymbol{v}_\mu)\|^2 + \|\boldsymbol{\sigma}'_l(\tilde{\mathbf{x}}|\tilde{y} = c) - \mathcal{N}(\boldsymbol{\sigma}'_l(\hat{\mathbf{x}}|\hat{y} = c), \boldsymbol{v}_\sigma)\|^2, \quad (7)$$

where $\boldsymbol{v}_\mu = 0.5$ and $\boldsymbol{v}_\sigma = 1.0$ are used to control the distortion degrees of mean and variance. For each synthetic data $\tilde{\mathbf{x}}$, its target is sampled from a Gaussian distribution centered on the class centroid of $\tilde{\mathbf{x}}$. As a result, our BNS-distorted loss provides diverse distorted centroids which prevent the BNS of per synthetic data from overfitting its centroid. And thus, we further retain the intra-class incohesion.

Our experiments show that the BNS-distorted loss can retain the inter-class separation to some extent since the distorted centroid for synthetic data is centered on the corresponding class centroid. However, it is hard to manually model the Gaussian noise exactly such that the inter-class separability and intra-class incohesion can be preserved simultaneously. Thus, both BNS-centralized loss and BNS-distorted loss are necessary in the experiment.

Model Quantization

Classification. To make full use of the available data, both calibration images and synthetic images are used to fine-tune the quantized model Q , which can be realized through the cross-entropy loss:

$$\mathcal{L}_{\text{CE}}^Q = \mathbb{E}_{(\mathbf{x}, y) \sim D \cup \{(\tilde{\mathbf{x}}, \tilde{y})\}} [\text{CE}(Q(\mathbf{x}), y)]. \quad (8)$$

Distillation. It is possible that the synthetic image will not include corresponding class-specific features. As a result, \tilde{y} may be unreliable. Thus, we apply knowledge distillation (KD) (Hinton, Vinyals, and Dean 2015) to transfer the outputs of full-precision model F to quantized model Q so that even though the synthetic image may have an inaccurate label, Q can still be correctly optimized by learning the soft target provided by F . Moreover, KD is also beneficial to the

learning of calibration data. The KD loss is defined by the Kullback-Leibler distance $\text{KL}(\cdot, \cdot)$ as:

$$\mathcal{L}_{\text{KD}}^Q = \mathbb{E}_{(\mathbf{x}, y) \sim D \cup \{(\tilde{\mathbf{x}}, \tilde{y})\}} [\text{KL}(Q(\mathbf{x}), F(\mathbf{x}))]. \quad (9)$$

Training Process

The training of our method consists of updating the generator G and the quantized model Q , where Q is obtained by quantizing the pre-trained full-precision model F . G produces a set of synthetic images while Q is trained with the aid of synthetic images and calibration images. We also emphasize that the F is fixed without any updating during the whole training process.

Updating Generator G . With a random Gaussian noise \tilde{z} conditional on label \tilde{y} as its input, the generator G synthesizes an image $\tilde{\mathbf{x}} = G(\tilde{z}|\tilde{y})$, which is then used for classification of Eq. (4) and preserving distribution of training set including the coarse alignment of Eq. (3), inter-class separation of Eq. (6) and intra-class incohesion of Eq. (7). Thus, the overall loss for the generator G can be derived as:

$$\mathcal{L}^G = \alpha_1 \cdot \mathcal{L}_{\text{CE}}^G + \alpha_2 \cdot \mathcal{L}_{\text{BNS}}^G + \alpha_3 \cdot \mathcal{L}_{\text{D-BNS}}^G + \alpha_4 \cdot \mathcal{L}_{\text{C-BNS}}^G, \quad (10)$$

where the $\alpha_1, \alpha_2, \alpha_3$ and α_4 are the trade-off parameters.

Updating Quantized Model Q . The quantized model Q takes the synthetic data and calibration data as its inputs, and then the classification loss of Eq. (8) and distillation loss of Eq. (9) are constructed to retain the performance. Thus, the overall loss for the quantized model Q can be derived as:

$$\mathcal{L}^Q = \mathcal{L}_{\text{CE}}^Q + \alpha_5 \cdot \mathcal{L}_{\text{KD}}^Q, \quad (11)$$

where α_5 is a trade-off parameter.

Experimentation

Implementation Details

We choose to quantize ResNet-18 (He et al. 2016), MobileNetV1 (Howard et al. 2017), MobileNetV2 (Sandler et al. 2018) and RegNet-600MF (Radosavovic et al. 2020). All experiments are conducted on the challenging ImageNet with 1.2 million training images and 50,000 validation images from 1,000 classes (Russakovsky et al. 2015). The calibration dataset consists of 1,000 images including one image per class. We report the top-1 accuracy and the code is implemented using Pytorch (Paszke et al. 2019).

For ease of implementation, we directly borrow the generator from GDFQ (Xu et al. 2020) to produce synthetic images. The initial learning rates for the generator and quantized network are set to 10^{-3} and 10^{-6} respectively. For the generator, the optimizer is Adam (Kingma and Ba 2014) with 0.9 as the momentum and the learning rate are multiplied by 0.1 every 100 epochs. For the quantized network, the optimizer is SGD with Nesterov (Nesterov 1983) with 10^{-4} as the weight decay and we adjust the learning rate using the cosine annealing (Loshchilov and Hutter 2016). Before formal training, we set up a warm-up updating of the generator G for 50 epochs. Then, a total of 350 epochs are used to update the generator G and quantized model Q .

	Methods	ResNet-18	MobileNetV1	MobileNetV2	RegNet-600MF
Settings	Full precision	71.47	73.39	72.49	73.71
W5A5, F8L8	ACIQ-Mix (Banner et al. 2019)	68.34	52.34	61.74	69.53
	AdaQuant (Hubara et al. 2020)	68.56	-	65.19	-
	Bit-Split (Wang et al. 2020)	69.10	-	-	-
	BRECQ (Li et al. 2021)	70.60	70.16	70.83	73.38
	FDDA(Ours)	70.86	71.76	71.99	73.99
W4A4, F8L8	ACIQ-Mix (Banner et al. 2019)	67.0	5.06	39.49	54.22
	AdaQuant (Hubara et al. 2020)	67.50	-	34.95	-
	Bit-Split (Wang et al. 2020)	67.56	-	-	-
	BRECQ (Li et al. 2021)	69.60	63.66	66.57	68.33
	FDDA(Ours)	69.76	65.76	69.32	70.33
W5A5, F5L5	ACIQ-Mix (Banner et al. 2019)	66.80	51.65	60.42	69.13
	AdaQuant (Hubara et al. 2020)	68.19	-	63.61	-
	Bit-Split (Wang et al. 2020)	68.88	-	-	-
	BRECQ (Li et al. 2021)	70.27	66.51	70.26	72.78
	FDDA(Ours)	70.56	70.26	71.63	73.62
W4A4, F4L4	ACIQ-Mix (Banner et al. 2019)	57.47	4.68	34.84	51.74
	AdaQuant (Hubara et al. 2020)	63.45	-	34.64	-
	Bit-Split (Wang et al. 2020)	67.49	-	-	-
	BRECQ (Li et al. 2021)	67.94	57.11	63.64	66.17
	FDDA(Ours)	68.74	63.75	68.38	68.96

Table 1: Comparisons with existing post-training quantization methods. WBAB indicates the weights and activations are quantized to B-bit while FBLB indicates the first layers and last layers are quantized to B-bit.

Experimental Results

Comparison with Baseline. We first compare with the zero-shot GDFQ (Xu et al. 2020), since the data synthesis of our FDDA is built upon the framework of GDFQ.

Tab. 2 displays our experimental results when all layers of ResNet-18 (He et al. 2016) are quantized to 4-bit. As can be seen, the accuracy of the full-precision model decreases from 71.47% to around 68.24% when the training-aware quantization, which requires all training data, is applied. Regarding GDFQ which only considers the synthetic data for fine-tuning the quantized model, performance severely degenerates to 60.60%. Such poor performance disables the application of GDFQ. Given the calibration dataset, GDFQ can increase to 65.48%, well demonstrating the correctness of our motive in combining real calibration dataset with synthetic data. Nevertheless, the coarse BNS alignment in GDFQ fails to model the fine-grained properties of inter-class separability and intra-class incohesion. When solved by our FDDA, the performance further increases to 68.74%, better than the training-aware quantization. This result demonstrates the efficacy of our BNS-centralized loss and BNS-distorted loss in synthesizing better images.

In our settings, we assume to have access to the image labels. However, these labels are sometimes not available in real life. Luckily, the pre-trained full-precision model can be used to predict these labels. In Tab. 2, we also report the performance of our FDDA, *i.e.*, 68.68%, using predicted labels. The slight drops are attributed to some of the misclassified labels. Nevertheless, our FDDA without real labels still maintains better performance than GDFQ with real images, well demonstrating the importance of preserving the fine-grained inter-class separability and intra-class incohesion when learning to synthesize images.

Method	Acc. (%)
Full precision	71.47
TAQ	68.24
GDFQ	60.60
GDFQ + C	65.48
GDFQ + C + F (FDDA)	68.74
FDDA + w/o label	68.68

Table 2: Comparison with baseline when all layers of ResNet-18 are quantized to 4-bit. TAQ denotes training-aware quantization. “C” indicates the calibration dataset. “F” represents our fine-grained data distribution alignment.

Comparison with Competitors. We then compare with the recent studies on post-training quantization (Banner et al. 2019; Hubara et al. 2020; Wang et al. 2020; Li et al. 2021). The quantized networks include ResNet-18 (He et al. 2016), MobileNetV1 (Howard et al. 2017), MobileNetV2 (Sandler et al. 2018) and RegNet-600MF (Radosavovic et al. 2020). All networks are quantized to the low precision 5-bit and 4-bit. Besides, to show the advantage of our FDDA, we quantize the first and last layers to 8-bit and lower precision (5-bit or 4-bit). Tab. 1 shows the experimental results.

When the first and last layers of full-precision models are quantized to 8-bit (F8L8), both our FDDA and recent SOTA BRECQ (Li et al. 2021) can retain a high performance of the full-precision models regardless of 5-bit (W5A5) or 4-bit (W4A4) weights and activations in other layers. Besides, Comparing to BRECQ, our FDDA obtains performance gains by 0.26%, 1.60%, 1.16% and 0.61% when quantizing ResNet-18, MobileNetV1, MobileNetV2 and ResNet-600MF to W5A5, while they are 0.16%, 2.10%, 2.75% and 2.00% when quantized to W4A4. We observe that our

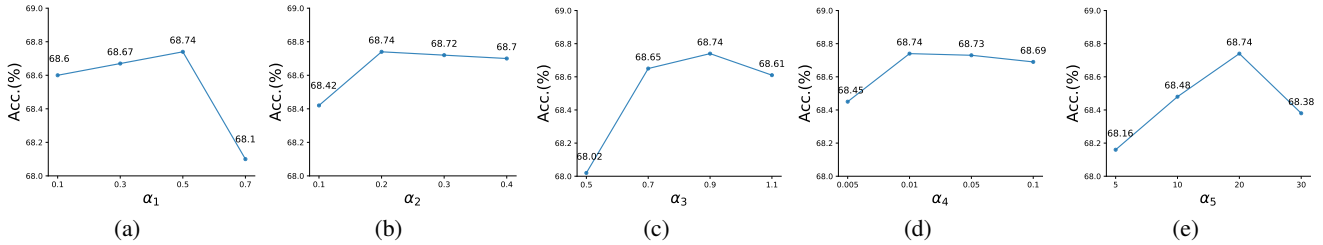


Figure 4: Influence of the trade-off parameters.

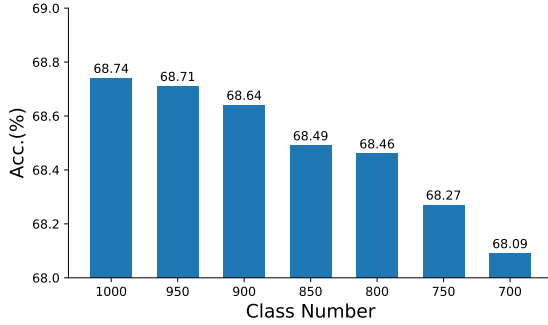


Figure 5: Influence of available classes.

FDDA retains better performance than BRECQ when quantizing light-weight models such as MobileNets, particularly when lower precision, such as 4-bit, is performed.

When the first and last layers of full-precision models are quantized to lower precision (F5L5 or F4L4) as well, we can see that our FDDA outperforms BRECQ by margins. Specifically, our FDDA increases the performance of BRECQ in W5A5 by 0.29%, 3.75%, 1.37% and 0.84% *w.r.t.* ResNet-18, MobileNetV2, MobileNetV2 and ResNet-600MF, and the performance gains are 0.80%, 6.64%, 4.74%, 2.79% in the case of W4A4. These results well verify our statement in the introduction section that the performance improvements of existing studies are usually built on the premise that the first and last layers are quantized to higher precision, and also demonstrates the effectiveness of our combining real calibration dataset with synthetic data to enhance the performance of post-training quantization.

Ablation Studies

In this section, we give an in-depth study on the influence of hyper-parameters in this paper including the trade-off parameters in Eq. (10) and Eq. (11), and the number of available images in the calibration dataset. All experiments are conducted by quantizing all layers of ResNet-18 to 4-bit.

Trade-off Parameters. We first display the influence of different trade-off parameters in Fig. 4. The α_1 , α_2 , α_3 , and α_4 from Eq. (10) balance different losses in updating the generator while α_5 from Eq. (11) balances the losses in updating the quantized model. From Fig. 4, we can see that the optimal configurations of these parameters are $\alpha_1 = 0.5$, $\alpha_2 = 0.2$, $\alpha_3 = 0.9$, $\alpha_4 = 0.01$ and $\alpha_5 = 20$, which are also our settings for all the aforementioned experiments. Though

they might not be the optimal for all networks, we find these configurations already bring better performance than the recent state-of-the-arts. Also, we observe that $\alpha_4 << \alpha_3$ in which α_3 and α_4 respectively balance the importance of the proposed BNS-distorted loss and BNS-centralized loss. This is due to the distorted centroid for synthetic data is centered on the corresponding class centroid, thus the BNS-distorted loss can retain the inter-class separation to some extent, which partly relieves the involvement of BNS-centralized loss and leads to a small α_4 .

Effect of Available Classes. The calibration dataset consists of 1,000 images including one image per class. However, some class information might be missing in real-world applications. Consequently, the corresponding images are not available for our fine-grained BNS alignment. In Fig. 5, we study the influence of available classes on our final performance. No doubt that performance drops as the available classes decrease. Nevertheless, comparing to BRECQ which obtains 67.94% top-1 accuracy (see Tab. 1), our FDDA still maintains a higher performance of 68.09% even when only 700 classes are available. The good performance can be attributed to two reasons. On one hand, synthetic data benefits post-training quantization. On the other hand, the fine-grained data alignment helps to synthesize better images for fine-tuning the quantized model even though some classes are missing.

Conclusion

In this paper, we proposed a fine-grained data distribution alignment (FDDA) to solve the insufficient data problem in post-training quantization. We observed two important BNS properties of the inter-class separation and intra-class incohesion in the deep layers of network. To retain these two fine-grained distribution information, we respectively proposed a BNS-centralized loss and a BNS-distorted loss. Using a real image from the calibration dataset as the centroid of each class, the BNS-centralized loss constrains the BNS of synthetic data to be close to the BNS of its class centroid, while the BNS-distorted loss introduces Gaussian noise to distort the class centroid for the purpose of incohesion. By retaining these two properties in the synthetic data, our FDDA shows its superiority over the state-of-the-art competitors on ImageNet, particularly when the first and last layers of networks are also quantized to low precision.

References

Banner, R.; Nahshan, Y.; Soudry, D.; et al. 2019. Post training 4-bit quantization of convolutional networks for rapid-deployment. In *Proceedings of the Advances in Neural Information Processing Systems (NeurIPS)*, 7950–7958.

Cai, Y.; Yao, Z.; Dong, Z.; Gholami, A.; Mahoney, M. W.; and Keutzer, K. 2020. ZeroQ: A Novel Zero Shot Quantization Framework. In *Proceedings of the IEEE/CVF Conference on Computer Vision and Pattern Recognition (CVPR)*, 13169–13178.

Chen, H.; Wang, Y.; Xu, C.; Yang, Z.; Liu, C.; Shi, B.; Xu, C.; Xu, C.; and Tian, Q. 2019. Data-Free Learning of Student Networks. In *Proceedings of the IEEE/CVF International Conference on Computer Vision (ICCV)*, 3514–3522.

Choi, J.; Wang, Z.; Venkataramani, S.; Chuang, P. I.-J.; Srinivasan, V.; and Gopalakrishnan, K. 2018. PACT: Parameterized Clipping Activation for Quantized Neural Networks. *arXiv preprint arXiv:1805.06085*.

Fang, J.; Shafiee, A.; Abdel-Aziz, H.; Thorsley, D.; Georgiadis, G.; and Hassoun, J. H. 2020. Post-Training Piecewise Linear Quantization for Deep Neural Networks. In *Proceedings of the European Conference on Computer Vision (ECCV)*, 69–86.

Gholami, A.; Kim, S.; Dong, Z.; Yao, Z.; Mahoney, M. W.; and Keutzer, K. 2021. A Survey of Quantization Methods for Efficient Neural Network Inference. *arXiv preprint arXiv:2103.13630*.

Goodfellow, I. J.; Pouget-Abadie, J.; Mirza, M.; Xu, B.; Warde-Farley, D.; Ozair, S.; Courville, A.; and Bengio, Y. 2014. Generative Adversarial Nets. In *Proceedings of the Advances in Neural Information Processing Systems (NeurIPS)*, 2672–2680.

Han, S.; Pool, J.; Tran, J.; Dally, W. J.; et al. 2015. Learning both Weights and Connections for Efficient Neural Network. In *Proceedings of the Advances in Neural Information Processing Systems (NeurIPS)*, 1135–1143.

Haroush, M.; Hubara, I.; Hoffer, E.; and Soudry, D. 2020. The Knowledge Within: Methods for Data-Free Model Compression. In *Proceedings of the IEEE/CVF Conference on Computer Vision and Pattern Recognition (CVPR)*, 8494–8502.

He, K.; Zhang, X.; Ren, S.; and Sun, J. 2016. Deep Residual Learning for Image Recognition. In *Proceedings of the IEEE/CVF Conference on Computer Vision and Pattern Recognition (CVPR)*, 770–778.

Hinton, G.; Vinyals, O.; and Dean, J. 2015. Distilling the Knowledge in a Neural Network. *arXiv preprint arXiv:1503.02531*.

Howard, A. G.; Zhu, M.; Chen, B.; Kalenichenko, D.; Wang, W.; Weyand, T.; Andreetto, M.; and Adam, H. 2017. MobileNets: Efficient Convolutional Neural Networks for Mobile Vision Applications. *arXiv preprint arXiv:1704.04861*.

Hubara, I.; Nahshan, Y.; Hanani, Y.; Banner, R.; and Soudry, D. 2020. Improving Post Training Neural Quantization: Layer-wise Calibration and Integer Programming. *arXiv preprint arXiv:2006.10518*.

Hubara, I.; Nahshan, Y.; Hanani, Y.; Banner, R.; and Soudry, D. 2021. Accurate Post Training Quantization With Small Calibration Sets. In *Proceedings of the International Conference on Machine Learning (ICML)*, 4466–4475.

Kingma, D. P.; and Ba, J. 2014. Adam: A Method for Stochastic Optimization. In *Proceedings of the International Conference on Learning Representations (ICLR)*.

Krishnamoorthi, R. 2018. Quantizing deep convolutional networks for efficient inference: A whitepaper. *arXiv preprint arXiv:1806.08342*.

Kryzhanovskiy, V.; Balitskiy, G.; Kozyrskiy, N.; and Zurev, A. 2021. QPP: Real-Time Quantization Parameter Prediction for Deep Neural Networks. In *Proceedings of the IEEE/CVF Conference on Computer Vision and Pattern Recognition (CVPR)*, 10684–10692.

Li, Y.; Gong, R.; Tan, X.; Yang, Y.; Hu, P.; Zhang, Q.; Yu, F.; Wang, W.; and Gu, S. 2021. BRECQ: Pushing the Limit of Post-Training Quantization by Block Reconstruction. In *Proceedings of the International Conference on Learning Representations (ICLR)*.

Lin, M.; Ji, R.; Xu, Z.; Zhang, B.; Wang, Y.; Wu, Y.; Huang, F.; and Lin, C.-W. 2020. Rotated Binary Neural Network. In *Proceedings of the Advances in Neural Information Processing Systems (NeurIPS)*, 7474–7485.

Liu, X.; Ye, M.; Zhou, D.; and Liu, Q. 2021. Post-training Quantization with Multiple Points: Mixed Precision without Mixed Precision. In *Proceedings of the AAAI Conference on Artificial Intelligence (AAAI)*, 8697–8705.

Liu, Y.; Zhang, W.; and Wang, J. 2021. Zero-shot Adversarial Quantization. In *Proceedings of the IEEE/CVF Conference on Computer Vision and Pattern Recognition (CVPR)*, 1512–1521.

Loshchilov, I.; and Hutter, F. 2016. SGDR: Stochastic Gradient Descent with Warm Restarts. In *Proceedings of the International Conference on Learning Representations (ICLR)*.

Nagel, M.; Amjad, R. A.; Van Baalen, M.; Louizos, C.; and Blankevoort, T. 2020. Up or Down? Adaptive Rounding for Post-Training Quantization. In *Proceedings of the International Conference on Machine Learning (ICML)*, 7197–7206.

Nahshan, Y.; Chmiel, B.; Baskin, C.; Zheltonozhskii, E.; Banner, R.; Bronstein, A. M.; and Mendelson, A. 2019. Loss Aware Post-training Quantization. *arXiv preprint arXiv:1911.07190*.

Nesterov, Y. E. 1983. A method of solving a convex programming problem with convergence rate $O(k^2)$. In *Proceedings of the Russian Academy of Sciences (RAS)*, 543–547.

Paszke, A.; Gross, S.; Massa, F.; Lerer, A.; Bradbury, J.; Chanan, G.; Killeen, T.; Lin, Z.; Gimelshein, N.; Antiga, L.; et al. 2019. PyTorch: An Imperative Style, High-Performance Deep Learning Library. In *Proceedings of the Advances in Neural Information Processing Systems (NeurIPS)*, 8026–8037.

Radosavovic, I.; Kosaraju, R. P.; Girshick, R.; He, K.; and Dollár, P. 2020. Designing Network Design Spaces. In *Proceedings of the IEEE/CVF Conference on Computer Vision and Pattern Recognition (CVPR)*, 10428–10436.

Rousseeuw, P. J. 1987. Silhouettes: a graphical aid to the interpretation and validation of cluster analysis. *Journal of Computational and Applied Mathematics (JCAM)*, 20: 53–65.

Russakovsky, O.; Deng, J.; Su, H.; Krause, J.; Satheesh, S.; Ma, S.; Huang, Z.; Karpathy, A.; Khosla, A.; Bernstein, M.; et al. 2015. ImageNet Large Scale Visual Recognition Challenge. *International Journal of Computer Vision (IJCV)*, 115: 211–252.

Sandler, M.; Howard, A.; Zhu, M.; Zhmoginov, A.; and Chen, L.-C. 2018. MobileNetV2: Inverted Residuals and Linear Bottlenecks. In *Proceedings of the IEEE/CVF Conference on Computer Vision and Pattern Recognition (CVPR)*, 4510–4520.

van der Maaten, L.; and Hinton, G. 2008. Visualizing Data using t-SNE. *Journal of Machine Learning Research (JMLR)*, 9: 2579–2605.

Wang, P.; Chen, Q.; He, X.; and Cheng, J. 2020. Towards Accurate Post-training Network Quantization via Bit-split and Stitching. In *Proceedings of the International Conference on Machine Learning (ICML)*, 9847–9856.

Xu, S.; Li, H.; Zhuang, B.; Liu, J.; Cao, J.; Liang, C.; and Tan, M. 2020. Generative Low-bitwidth Data Free Quantization. In *Proceedings of the European Conference on Computer Vision (ECCV)*, 1–17.

Zhang, X.; Qin, H.; Ding, Y.; Gong, R.; Yan, Q.; Tao, R.; Li, Y.; Yu, F.; and Liu, X. 2021a. Diversifying Sample Generation for Accurate Data-Free Quantization. In *Proceedings of the IEEE/CVF Conference on Computer Vision and Pattern Recognition (CVPR)*, 15658–15667.

Zhang, Y.; Chen, H.; Chen, X.; Deng, Y.; Xu, C.; and Wang, Y. 2021b. Data-Free Knowledge Distillation for Image Super-Resolution. In *Proceedings of the IEEE/CVF Conference on Computer Vision and Pattern Recognition (CVPR)*, 7852–7861.